Macromolecules

Article

pubs.acs.org/Macromolecules

Highly Stable Polymer Solar Cells Based on Poly(dithienobenzodithiophene-*co*-thienothiophene)

Nara Shin,[†,‡] Hui-Jun Yun,[§] Youngwoon Yoon,[†] Hae Jung Son,[†] Sang-Yong Ju,[‡] Soon-Ki Kwon,*[,§] BongSoo Kim,*[,†,∥] and Yun-Hi Kim*[,⊥]

[†]Photo-electronic Hybrids Research Center, Korea Institute of Science and Technology (KIST), Seoul 136-791, Republic of Korea

[‡]Department of Chemistry, Yonsei University, Seoul 120-749, Republic of Korea

[§]School of Materials Science and Engineering, Engineering Research Institute, Gyeongsang National University, Jinju 660-701, Republic of Korea

[∥]Department of Science Education, Ewha Womans University, Seoul 120-750, Republic of Korea

[⊥]Department of Chemistry and RIGET, Gyeongsang National University, JinJu 600-701, Republic of Korea

Supporting Information

ABSTRACT: It is important to develop new donor (D)−acceptor (A) type low band gap polymers for highly stable polymer solar cells (PSCs). Here, we describe the synthesis and photovoltaic properties of two D−A type low band gap polymers. The polymers consist of dithienobenzodithiophene (DTBDT) moieties with expanded conjugation side groups as donors and 2-ethyl-1-(thieno[3,4-*b*]thiophen-2-yl)hexan-1-one (TTEH) or 6-octyl-5*H*-thieno[3′,4′:4,5]thieno[2,3-*c*]pyrrole-5,7(6*H*)-dione (DTPD) as acceptors to give pDTBDT-TTEH and pDTBDT-DTPD polymers, respectively. The pDTBDT-TTEH is quite flat, resulting in a highly crystalline film. In contrast, the pDTBDT-DTPD is highly twisted to yield an amorphous film. Photovoltaic devices based on pDTBDT-TTEH and pDTBDT-DTPD exhibited power conversion efficiencies (PCEs) of 6.74% and 4.44%, respectively. The PCE difference results mainly from morphological differences between the two polymer:$PC_{71}BM$ blend films; the pDTBDT-TTEH polymer formed a nanoscopically networked domains in the blend state, while the pDTBDT-DTPD polymer film contained aggregated domains with large phase separation between the polymer and $PC_{71}BM$ molecules. Importantly, we observed that pDTBDT-TTEH-based devices showed excellent stability—in air, retaining 95% of the initial PCE after storage for over 1000 h without encapsulation. The high stability of the pDTBDT-TTEH-based device was originated mainly by the crystalline nature of the pDTBDT-TTEH:$PC_{71}BM$ film. This work suggests that designing highly conjugated planar backboned polymers is crucial to improve not only the photovoltaic performance but also the stability of PSCs.

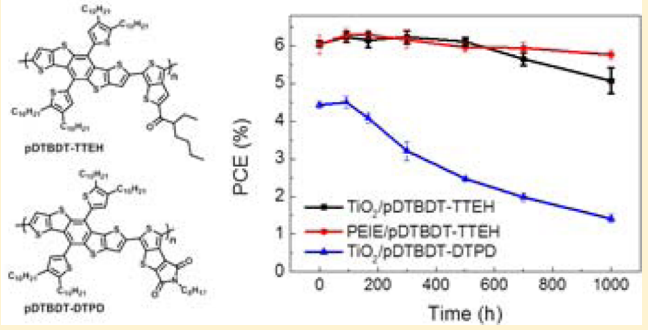

1. INTRODUCTION

Polymer solar cells (PSCs) have attracted considerable attention as renewable energy sources due to their unique advantages such as low cost, light weight, and the likelihood that they could be flexible even when manufactured at large area.[1−4] To date, the most promising PSCs require bulk-heterojunction (BHJ)-type photoactive layers, typically consisting of a low band gap conjugated polymer and a fullerene derivative.[5] Advances in PSC performance have resulted mainly from the development of new low band gap (LBG) polymers.[6−14] LBG polymers should have low optical band gaps to harvest photons from a broad spectrum of solar light. A second requirement is a lowest unoccupied molecular orbital (LUMO) energy level that ensures exciton dissociation at the polymer/fullerene interface and a deep highest occupied molecular orbital (HOMO) energy level that affords high open-circuit voltage (V_{oc}) and stability.[15−18] Lastly, high carrier mobility is beneficial for efficient charge collection.[19−23]

To synthesize high performance LBG polymers, benzo[1,2-*b*;4,5-*b*′]dithiophene (BDT) has been widely used as the electron-rich donor unit. For example, copolymerization of BDT with various acceptor units, such as electron-withdrawing group-attached thieno[3,4-*b*]dithiophene (TT), diketo-pyrrolopyrrole (DPP), benzothiadiazole (BZ), and *N*-alkyl-thieno[3,4-*c*]pyrrole-4,6-dione (TPD), has yielded polymers displaying promising photovoltaic performances.[24−29] Recently, large heteroacenes have also been employed in high-performance PSCs, as they provide many advantages including enhanced charge carrier mobility caused by increased interchain

Received: March 11, 2015
Revised: May 20, 2015
Published: June 8, 2015

DOI: 10.1021/acs.macromol.5b00514
Macromolecules 2015, 48, 3890−3899

$\pi-\pi$ stacking via large planar π-conjugated structures; these polymers are also predicted to yield narrow energy band gaps by effective overlapping of the expanded π-system.[30−33] In addition, increased effective conjugation length in heteroacene-incoporating polymers decreases reorganization energy of the polymeric system, facilitating exciton separation into free charge carriers.[35,36] Because of these advantages, we reported the synthesis of LBG polymers utilizing derivatives of the five-membered heteroacene, dithienobenzodithiophene (DTBDT) with dialkoxy or dialkythienyl substituents.[37] The introduced dialkylthienyl side groups solved problems with increased solubility and a lower HOMO energy level than the dialkoxybenzodithiophene, which was ascribed to the slightly distorted conjugation between the DTBDT unit and dialkylthienyl side groups. These favorable characteristics resulted in a PCE of up to 5.1% with a high V_{oc} without sacrificing charge transport properties.

To improve the photovoltaic performance of these polymers, we now report the polymerization of the dithienobenzodithiophene (DTBDT) derivative with the acceptors 2-ethyl-1-(thieno[3,4-*b*]thiophen-2-yl)hexan-1-one (TTEH)[10] or *N*-octyl-2,7-dithia-5-azacyclopenta[*a*]pentalene-4,6-dione (DTPD),[11] yielding pDTBDT-TTEH and pDTBDT-DTPD polymers, respectively. Both polymers had a low band gap of ∼1.6 eV and low HOMO levels. pDTBDT-TTEH-based devices (PCE = 6.74%) outperformed pDTBDT-DTPD-based devices (PCE = 4.44%) and also demonstrated higher stability in air. This article describes the origin of the performance difference between the two polymer-based devices and correlates their photovoltaic properties and air stability with polymer chemical structure.

2. EXPERIMENTAL SECTION

Materials and Synthesis. *Material Characterization.* ^{1}H NMR and ^{13}C NMR spectra were recorded with a Bruker Advance-300 and -500 spectrometer. The thermal analysis were performed on a TA TGA 2100 thermogravimetric analyzer in a nitrogen atmosphere at a rate of 10 °C/min. Differential scanning calorimetry (DSC) was conducted under nitrogen on a TA Instruments 2100 DSC. The sample was heated with 10 °C/min from 30 to 300 °C. UV−vis absorption spectra were measured by a UV-1650PC spectrophotometer. Molecular weights and polydispersities of the copolymers were determined by gel permeation chromatography (GPC) analysis with polystyrene standard calibration (Waters high-pressure GPC assembly Model M515 pump, μ-Styragel columns of HR4, HR4E, and HR5E, with 500 and 100 Å, refractive index detectors; solvent: chloroform). Cyclic voltammetry (CV) was performed on an EG and G Parc model 273 Å potentiostat/galvanostat system with a three-electrode cell in a solution of 0.1 M tetrabutylammonium hexafluorophosphate in acetonitrile at a scan rate of 50 mV/s. The polymer films were coated on a platinum (Pt) electrode by dipping the electrode into the corresponding polymer solutions, which was then dried under nitrogen. Another Pt wire was used as the counter electrode, and an Ag/Ag$^+$ electrode was used as the reference electrode. The reference electrode potential was calibrated with respect to the ferrocene/ferrocenium (Fc/Fc$^+$), which was assumed to be −4.8 eV. Atomic force microscopy (AFM) images of the polymer:$PC_{71}BM$ blend films were recorded on a XE-100 (Park systems) with an AC160-TS cantilever in the tapping mode. AFM samples were fabricated in the same method for OPV devices without TiO_2/Al or MoO_3/Ag deposition. Photoluminescence (PL) spectra of the polymer:$PC_{71}BM$ blends were obtained on a Horiba Jobin Yvon spectrometer (iHR320, FL 3-1 iHR, S1 detector). Transmission electron microscopy (TEM) images were taken on Philips CM30 microscope at an operating voltage of 300 keV. For TEM experiments, the polymer:$PC_{71}BM$ blend films spin-coated on the ITO/PEDOT:PSS substrates were floated in water and then lifted on a carbon-coated square mesh copper grid (#200 mesh). The electronic structures and conformations of model compounds of polymer backbone in study were estimated by density functional theory (DFT) calculations. The model compound consisting of three repeating units of polymers were geometrically optimized to an energy minimum using Gaussian 09 at the DFT B3LYP level with a 6-31+G(d,p) basis set. To save the calculation time, all the alkyl chains were shortened to methyl groups.

Material Preparation. All reactions were carried out in a nitrogen atmosphere using the usual Schlenk techniques. All chemical reagents were purchased from Aldrich, TCI, and Umicore and used as received unless otherwise specified. All solvents were further purified prior to use. 2-Ethyl-1-(thieno[3,4-*b*]thiophen-2-yl)hexan-1-one,[10] 6-octyl-5*H*-thieno[3′,4′:4,5]thieno[2,3-*c*]pyrrole-5,7(6*H*)-dione,[11] and 5,10-bis-(4,5-didecylthiophene-2-yl)benzo[1,2-*b*;4,5-*b*′]diithieno[3,2-*b*]-thiophene[37] were prepared according to the literature procedures (Figures S1−S3).

Polymerization of pDTBDT-TTEH. The polymer was prepared using a palladium-catalyzed Stille coupling reaction. Compound **1** (0.094 g, 0.221 mmol) and compound **3** (0.3 g, 0.221 mmol) were dissolved in dry chlorobenzene (4.5 mL). After degassing under nitrogen for 60 min, $Pd_2(dba)_3$ (4.06 mg, 0.00443 mmol) and P(*o*Tol)$_3$ (5.39 mg, 0.01773 mmol) were added to the mixture, which was then stirred for 48 h at 110 °C. 2-Bromothiophene and tributyl(thiophen-2-yl)stannane were injected sequentially into the reaction mixture for end-capping, and the solution was stirred for 6 h after each addition. The reaction mixture was precipitated in methanol. The crude polymer was collected by filtration and purified by Soxhlet extraction with methanol, acetone, hexane, toluene, and chloroform, successively. The pDTBDT-TTEH was obtained by precipitation of chloroform fraction in methanol. Yield: 75%. (M_n = 37 000 Da, M_w = 80 000 Da, PDI = 2.16*Đ*). ^{1}H NMR ($CDCl_3$, 500 MHz), δ (ppm): δ 7.69−7.39 (broad, 3H), 6.97−6.94 (broad, 2H), 4.07−3.98 (broad, 21H), 1.96−1.18 (m, 60 H), 1.03−0.85 (m, 18 H) (Figure S4). Element Anal. Calcd: C, 70.64; H, 8.27; N, 0; S, 19.85. Found: C, 71.69; H, 8.29; N, 0.00; S, 19.90.

Polymerization of pDTBDT-DTPD. pDTBDT-DTPD polymer was prepared in the same way as described for pDTBDT-TTEH using compound **2** (0.106 g, 0.221 mmol), compound **3** (0.3 g, 0.221 mmol), $Pd_2(dba)_3$ (4.06 mg, 0.004 43 mmol), and P(*o*Tol)$_3$ (5.39 mg, 0.017 73 mmol). The pDTBDT-DTPD was obtained by precipitation of chloroform fraction in methanol. Yield: 55% (M_n = 25 000 Da, M_w = 42 000 Da, PDI = 1.68*Đ*). ^{1}H NMR ($CDCl_3$, 500 MHz), δ (ppm): 7.52−7.39 (broad, 2H), 7.18−7.05 (broad, 2H), 4.04−3.94 (broad, 18H), 1.47−1.13 (m, 68 H), 1.03−0.85 (m, 15 H) (Figure S5). Element Anal. Calcd: C, 69.16; H, 8.22; N, 1.05; S, 19.18. Found: C, 69.29; H, 8.25; N, 1.04; S, 19.22.

Device Fabrication. Indium tin oxide (ITO) glass substrates were cleaned in a bath of isopropanol, acetone, and isopropanol for 10 min each with sonication sequentially and dried under a blow of nitrogen. The substrates were further cleaned with UV ozone for 20 min. PEDOT:PSS solution was purchased from Baytron, H.C. Starck (AI4083), and diluted with methanol (1:1 volume ratio). The diluted PEDOT:PSS solution was spin-cast at a speed of 4000 rpm for 35 s to give a 30 nm thick PEDOT:PSS layer. The PEDOT:PSS-coated ITO substrates were dried in a vacuum oven at 120 °C for 10 min. Polymer:$PC_{71}BM$ blend solutions (25 mg/mL) were prepared by dissolving a polymer and $PC_{71}BM$ (used as received from EM-Index) in chlorobenzene containing 3 vol % of 1,8-diiodooctane (DIO) with a weight ratio of 1:1.5. The blend solutions were then spin-cast onto ITO/PEDOT:PSS substrates at 3000 rpm for 35 s and dried on a hot plate at 70 °C for 20 min. Spin-casting TiO_2 nanoparticles in ethanol at 4000 rpm on top of the active layer yielded TiO_2 nanoparticle layers with a thickness of 10 nm. Finally, 100 nm thick aluminum was vacuum-deposited on ITO/PEDOT:PSS/polymer:$PC_{71}BM$/TiO_2 films through a shadow mask at a base pressure of 3×10^{-6} Torr with a deposition rate of 5 Å/s. To fabricate inverted type devices, 0.4 wt % TiO_2 nanoparticles in ethanol was first spin-cast at 4000 rpm on top of the cleaned ITO substrate, yielding TiO_2 nanoparticle layers

DOI: 10.1021/acs.macromol.5b00514
Macromolecules 2015, 48, 3890−3899

Scheme 1. Synthetic Routes to pDTBDT-TTEH and pDTBDT-DTPD

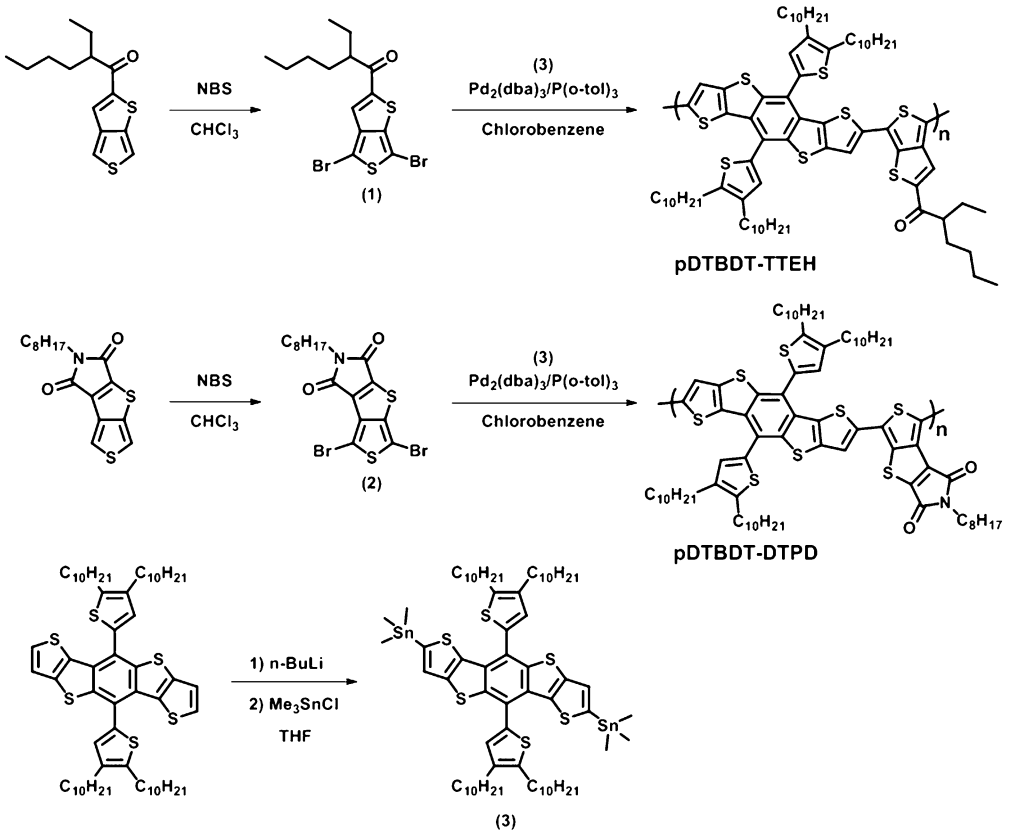

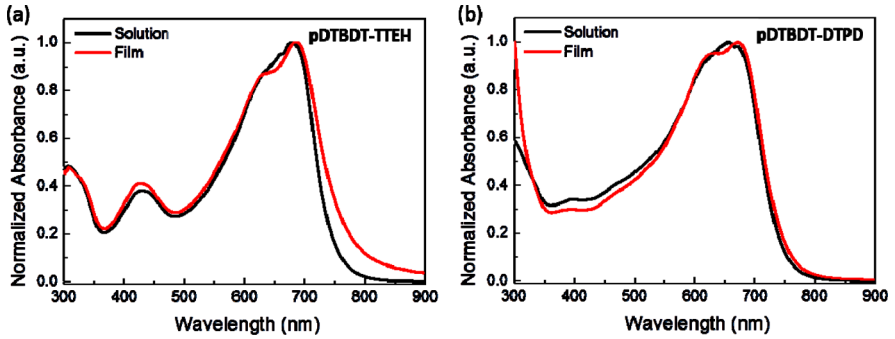

Figure 1. (a) UV−vis absorption spectra of the pDTBDT-TTEH and pDTBDT-DTPD polymers in solution and in film states.

with a thickness of ∼10 nm. Polymer:$PC_{71}BM$ blend solutions were prepared and spin-cast onto the TiO_2/ITO substrates as above described. Then, 5 nm thick molybdenum trioxide (MoO_3) layer was vacuum-deposited with a deposition rate of 0.1 Å/s and 100 nm thick silver was finally vacuum-deposited through a shadow mask at a base pressure of 3×10^{-6} Torr with a deposition rate of 5 Å/s. An active area of ITO/PEDOT:PSS/polymer:$PC_{71}BM$/TiO_2/Al and ITO/TiO_2/polymer:$PC_{71}BM$/MoO_3/Ag was 4×5 mm^2. Seven devices were fabricated, and their electrical properties were measured and averaged for each polymer-based device.

Current density versus voltage ($J-V$) characteristics were recorded on a Keithley model 2400 source measuring unit. A class-A solar simulator with a 150 W xenon lamp (Yamashita Denso Corp.) served as a light source. Its light intensity was adjusted to AM 1.5 G 1 sunlight intensity (100 mW/cm^2) using a NREL-calibrated silicon photodiode G425 with a KG-5 filter. External quantum efficiency (EQE) was measured as a function of wavelength from 300 to 1100 nm on incident photon-to-current conversion equipment (PV Measurement Inc.). Calibration was performed using a NIST-calibrated silicon photodiode G425 as a standard. Solar cell performances were measured with a mask covering all edges and the backside of the device. For the stability test, devices were stored in open air without encapsulation, and all the electrical measurements were done in air.

3. RESULTS AND DISCUSSION

Synthetic routes for both polymers are depicted in Scheme 1, and synthetic procedures are described in the Experimental Section. Monomers were prepared according to the literature procedures.[10,11,37] Polymerization was carried out by palladium-catalyzed Stille coupling. The polymers were purified by Soxhlet extraction in acetone, hexane, and chloroform, and the chloroform fraction was collected. The chemical structures of synthesized polymers were confirmed by NMR spectroscopy. pDTBDT-TTEH and pDTBDT-DTPD have good solubility in common organic solvents such as chloroform, chlorobenzene, and dichlorobenzene. Number-average molecular weights of pDTBDT-TTEH and pDTBDT-DTPD were estimated to be 37 and 25 kDa with polydisprsity indices of 2.16Đ and 1.68Đ,

DOI: 10.1021/acs.macromol.5b00514
Macromolecules 2015, 48, 3890−3899

respectively. The thermal properties of the polymers were studied by thermogravimetry analysis (TGA) and differencial scanning calorimetry (DSC) at a heating rate of 10 °C/min under a nitrogen atmosphere. Both pDTBDT-TTEH and pDTBDT-DTPD polymers showed good thermal stability, with 5% weight loss at 326 and 343 °C, respectively (Figure S6), and displayed no thermal transition in the range of 50−300 °C by DSC.

The light absorption of polymers in solution and as films was examined by UV−vis absorption spectroscopy (Figure 1). The spectrum of pDTBDT-TTEH included a peak at 676 nm in solution, which was red-shifted to 683 nm in the film state. The absorption spectrum of pDTBDT-DTPD included a peak at 658 nm in solution, red-shifted to 671 nm in the film. Though the absorption peaks were different in both states, the overall absorptions were nearly the same. Optical band gaps were determined to be 1.63 and 1.66 eV for pDTBDT-TTEH and pDTBDT-DTPD, respectively, from the absorption onsets of 760 and 748 nm.

Molecular energy levels were examined by cyclic voltammetry. Both polymers displayed clear oxidation curves (Figure 2a).

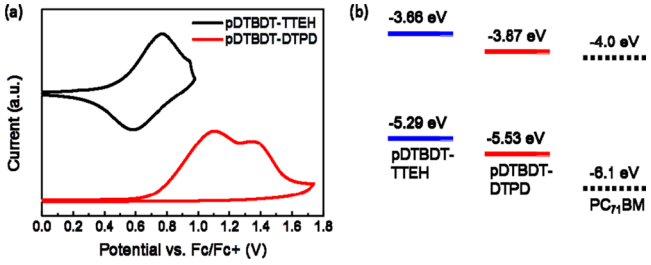

Figure 2. (a) Cyclic voltammograms and (b) HOMO/LUMO levels of pDTBDT-TTEH and pDTBDT-DTPD polymers. The HOMO/LUMO levels of $PC_{71}BM$ are shown together in (b).

From the onset of oxidation the HOMOs of pDTBDT-TTEH and pDTBDT-DTPD films were estimated to be −5.29 and −5.53 eV, respectively. The 0.24 eV deeper HOMO energy level of pDTBDT-DTPD indicates that the DTPD moiety is more electron-withdrawing than TTEH. LUMO levels were estimated by adding the HOMO levels to the optical band gaps to give −3.66 and −3.87 eV for pDTBDT-TTEH and pDTBDT-DTPD, respectively. The difference between the LUMO levels of pDTBDT-TTEH and $PC_{71}BM$ suggests that the energy offset is sufficient to produce efficient charge transfer/separation at polymer/$PC_{71}BM$ interfaces. However, the LUMO level of pDTBDT-DTPD is quite similar to that of $PC_{71}BM$ (−4.3 to −4.0 eV),[24−27] implying a low driving force for charge transfer/separation at the polymer/$PC_{71}BM$ interfaces. The pDTBDT-TTEH polymer has a lower HOMO level and a slightly broader light absorption than a previous reported PBDTTT-C and PBDTTT-C-T polymer consisting of di(2-ethylhexyl)oxybenzodithiophene and 4,8-bis(5-(2-ethylhexyl)thiophen-2-yl)benzo[1,2-*b*;4,5-*b*′]-dithiophene, respectively,[10,14] demonstrating the benefits of dithienyl-DTBDT moieties. These aspects also contribute to the slightly higher open-circuit voltage and higher short-circuit current of the pDTBDT-TTEH -based device than the PBDTTT-C-based device (see below).

The electronic structure, molecular geometries, and electronic transitions of polymers were obtained by quantum mechanical calculations using density functional theory (DFT). To expedite the calculations, three repeating units with methyl substitutions were used as model compounds, i.e., $(DTBDT\text{-}TTEH)_3$ and $(DTBDT\text{-}DTPD)_3$ in place of the pDTBDT-TTEH and pDTBDT-DTPD, respectively. Figure 3 shows the molecular orbitals and their energy levels and optimized geometries. Calculated energy levels are consistent with the experimentally determined UV−vis absorption and CV data, though the HOMO/LUMO energy levels are shifted slightly toward the vacuum level. The HOMO/LUMO levels of $(DTBDT\text{-}TTEH)_3$ lie higher than each corresponding level of $(DTBDT\text{-}DTPD)_3$. Surface plots of LUMO orbitals reveal that the DTBDT between the TTEH moieties effectively participates in the construction of the LUMO in the $(DTBDT\text{-}TTEH)_3$, whereas DTPD moieties contribute exclusively to the formation of the LUMO orbital of $(DTBDT\text{-}DTPD)_3$. This difference can be explained by backbone planarity; the $(DTBDT\text{-}TTEH)_3$ molecule is quite flat, whereas $(DTBDT\text{-}DTPD)_3$ molecules are twisted at the connection between the DTBDT and DTPD moieties because of the steric hindrance between the thienyl groups (Figure 3c,d). Considering the limited conjugation of $(DTBDT\text{-}DTPD)_3$, its lower LUMO level suggests that DTPD is a stronger accepting group than TTEH.

The photovoltaic properties of pDTBDT-TTEH and pDTBDT-DTPD were evaluated in a normal device structure of ITO/PEDOT:PSS/polymer:$PC_{71}BM$/TiO_2/Al under AM 1.5 G 1 sun illumination of 100 mW/cm^2 intensity. Figure 4a shows the current density−voltage curves, and Table 1 summarizes the measured photovoltaic parameters. pDTBDT-TTEH and pDTBDT-DTPD devices displayed open-circuit voltages (V_{oc}) of 0.72 and 0.79 V, respectively, consistent with the relative HOMO levels of the polymers. The pDTBDT-TTEH device showed a high short-circuit current (J_{sc}) of 15.77 mA cm^{-2}, whereas the pDTBDT-DTPD device showed a low J_{sc} of 6.64 mA cm^{-2}. The fill factors (FFs) were 0.59 and 0.54 for the pDTBDT-TTEH and pDTBDT-DTPD devices, respectively. As a result, the maximum PCEs were 6.74% and 2.83% for the pDTBDT-TTEH and pDTBDT-DTPD devices, respectively. Figure 4b shows the external quantum efficiency (EQE) spectra. pDTBDT-TTEH devices showed a high EQE response of over 60% in the range 400−700 nm with a maximum of 67%, whereas pDTBDT-DTPD devices exhibited a relatively lower EQE response; spectra were consistent with the measured J_{sc} values. Considering the relative light absorption of polymers and $PC_{71}BM$s, EQE response from our polymers likely contributed more at higher wavelengths (>550 nm) while that from $PC_{71}BM$s was in the shorter wavelengths. Thus, pDTBDT-TTEH appears to be equally efficient in generating photocarriers as $PC_{71}BM$ while pDTBDT-DTPD appears to be less efficient. This result is supported by the relative energy level alignment, as found in CV experiments.

To unravel the origins of the higher J_{sc} and the higher PCE in the pDTBDT-TTEH device, compared with the pDTBDT-DTPD device, polymer:$PC_{71}BM$ blend films were characterized using grazing incidence X-ray diffraction (GIXD), transmission electron microscopy (TEM), atomic force microscopy (AFM), photoluminescence (PL) spectroscopy, and carrier mobility measurements. The crystallinity and chain orientation of polymers in the polymer:$PC_{71}BM$ blend films were first probed by GIXD (Figure 5a,b). pDTBDT-TTEH polymers in the pDTBDT-TTEH:$PC_{71}BM$ blend film appeared highly crystalline, whereas pDTBDT-DTPD polymers in the pDTBDT-

DOI: 10.1021/acs.macromol.5b00514
Macromolecules 2015, 48, 3890−3899

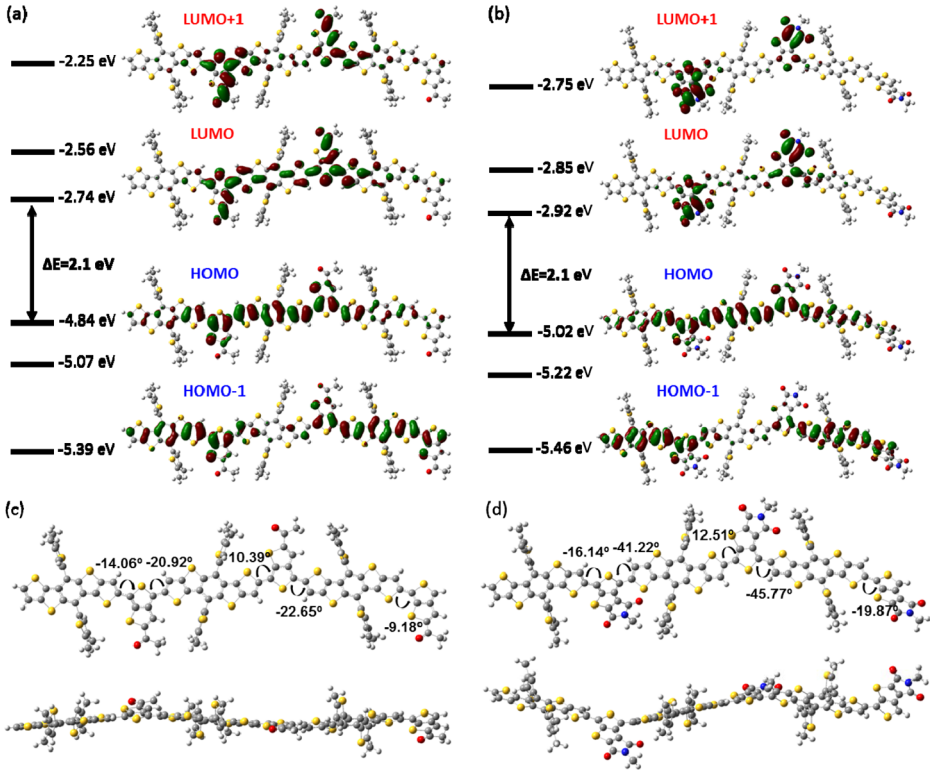

Figure 3. (a, b) Energy levels and molecular orbital surface plots of model compounds, $(DTBDT\text{-}TTEH)_3$ and $(DTBDT\text{-}DTPD)_3$, respectively. (c, d) Energy minimum molecular geometries of $(DTBDT\text{-}TTEH)_3$ and $(DTBDT\text{-}DTPD)_3$, respectively.

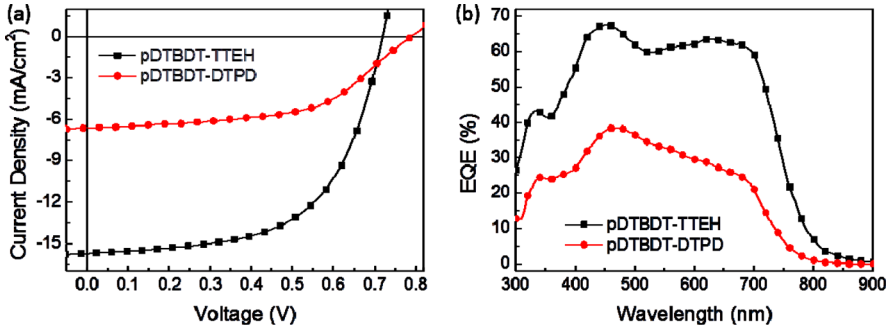

Figure 4. (a) Current density–voltage characteristics under simulated 100 mW/cm^2 AM1.5G illumination and (b) EQE spectra of the normal type pDTBDT-TTEH (black) and pDTBDT-DTPD (red) devices.

Table 1. Optical and Electrochemical Properties of the Polymers

sample	λ_{max} (nm) in solution	λ_{onset} (nm)[a] in film	E_g^{opt} [a] (eV)	HOMO[b] (eV)	LUMO[c] (eV)
pDTBDT-TTEH	676	760	1.63	−5.29	−3.66
pDTBDT-DTPD	683	748	1.66	−5.53	−3.87

[a]Optical band gap determined from UV–vis absorption onset. [b]Energy levels were determined by cyclic voltammetry. Standard three-electrode electrochemical cell in a 0.1 M Bu_4NPF_6 solution in acetonitrile at room temperature under a nitrogen atmosphere with a scanning rate of 100 mV/s. [c]Calculated from the HOMO + E_g^{opt}.

DTPD:$PC_{71}BM$ blend film were more amorphous. The crystallinity characteristics are strongly associated with polymer backbone structure; the planar pDTBDT-TTEH polymer formed a well-packed crystalline structure in film, whereas the twisted pDTBDT-DTPD polymer did not pack and remained less ordered. In addition, Figures 5b and 5c present respectively the out-of-plane profiles extracted along the q_z direction at q_y = 0.00 Å^{-1} and the in-plane profiles extracted along the q_y direction at q_z = 0.03 Å^{-1}. In the out-of-plane profiles, the pDTBDT-TTEH showed (100) and (200) peaks, corresponding to 19.9 Å, and pDTBDT-DTPD displayed only a (100) peak, corresponding to 18.3 Å. Comparing of the lamellar sizes to those of di(2-ethylhexyloxy)BDT-based polymers (~19 Å)[38,39] suggests that the pDTBDT-TTEH polymer containing longer linear decyl chains would have more interdigitation between the alkyl chains. However, the low lamellar size in the pDTBDT-DTPD:$PC_{71}BM$ blend films likely represents the averaged lamellar size of quite disordered polymer chains because of its low crystallinity. Moreover, a strong π–π stacking peak in the pDTBDT-TTEH:$PC_{71}BM$ blend film appeared at q_z = 1.71 Å^{-1} s, corresponding to 3.44 Å. The π–π stacking distance is even smaller value than the π–π stacking distances in BDT or heteroacene-based polymers.[28,36−39] Such low π–π

DOI: 10.1021/acs.macromol.5b00514
Macromolecules 2015, 48, 3890−3899

Table 2. PV Performance of the Normal Type Polymer:$PC_{71}BM$ Devices

sample	V_{oc} (V)	$J_{SC,I-V}$ (mA/cm^2)	$J_{SC,EQE}$ (mA/cm^2)	FF (%)	PCE (%)
pDTBDT-TTEH:$PC_{71}BM$	0.72	15.77	14.79	59.4	6.74 (av: 6.5)
pDTBDT-DTPD:$PC_{71}BM$	0.79	6.64	6.86	53.9	2.83 (av: 2.7)

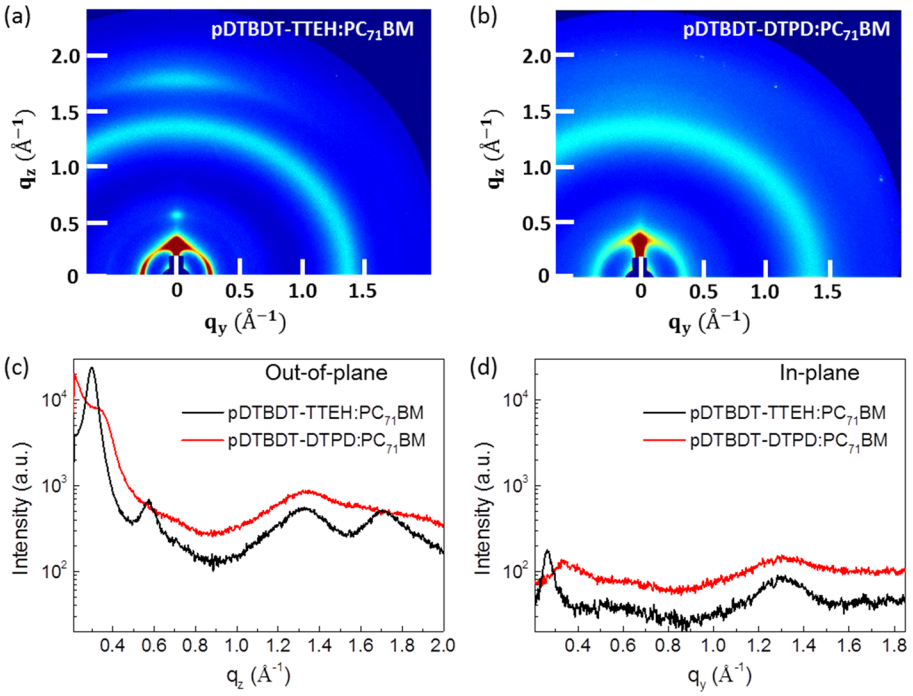

Figure 5. (a, b) GIXD images obtained from the pDTBDT-TTEH:$PC_{71}BM$ and pDTBDT-DTPD:$PC_{71}BM$ films. (c) Out-of-plane X-ray diffraction profiles extracted along the q_z direction at q_y = 0.00 Å^{-1}. (d) In-plane X-ray diffraction profiles along the q_y direction at q_z = 0.03 Å^{-1}.

stacking distance in the out-of-plane direction would assist hole transport in photovoltaic devices. In both the blend films, $PC_{71}BM$ domains displayed a radial distribution at q = 1.32 Å^{-1}, as observed previously.[39,41]

The phase separation between polymers and $PC_{71}BM$s in the blend films was characterized by TEM (Figure 6a,b) The pDTBDT-TTEH:$PC_{71}BM$ blend films exhibited homogeneous nanoscale phase separation between polymer domains, whereas pDTBDT-DTPD:$PC_{71}BM$ blend films displayed highly phase-separated morphology. In addition, AFM images of film surfaces support this characterization (Figure 6c,d). pDTBDT-TTEH:$PC_{71}BM$ film had a low root-mean-square (rms) value of 1.39 nm, consistent with evenly distributed nanoscale domains of polymer chains and $PC_{71}BM$s, while the pDTBDT-DTPD:$PC_{71}BM$ film had a larger rms value of 4.04 nm.

Photoluminescence (PL) quenching experiments were further conducted to confirm the interfacial interactions between polymer and $PC_{71}BM$ domains (Figure 7). The excitation light (λ_{ext} = 625 nm) was selected to selectively probe our polymers. Incident light on films of pure polymer and polymer:$PC_{71}BM$ blends generated PL spectra over the range 800−1400 nm. The pure pDTBDT-TTEH film exhibited slightly longer wavelength of PL peak at 797 nm than the pure pDTBDT-DTPD film ($\lambda_{PL,max}$ = 778 nm), in agreement with their light absorption onsets. While the PL intensities of the pure polymer films were similar, the pDTBDT-TTEH:$PC_{71}BM$ blend film showed more significantly reduced PL than the pDTBDT-DTPD:$PC_{71}BM$ blend film. The effective PL quenching in the pDTBDT-TTEH:$PC_{71}BM$ blend film

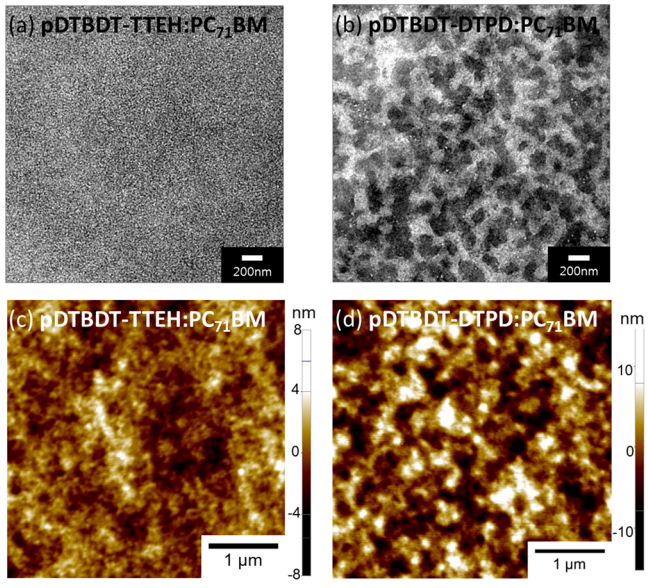

Figure 6. TEM images of (a) pDTBDT-TTEH:$PC_{71}BM$ and (b) pDTBDT-TTEH:$PC_{71}BM$. AFM images of (c) pDTBDT-TTEH:$PC_{71}BM$ and (d) pDTBDT-TTEH:$PC_{71}BM$. Blend films were spin-cast from a chlorobenzene solution containing the 3 vol % DIO additive.

suggests that the pDTBDT-TTEH polymer chains and the $PC_{71}BM$s were well-mixed. This fact is consistent with the observation of the uniform nanoscale phase separation in the TEM image and the enough LUMO−LUMO offset between

DOI: 10.1021/acs.macromol.5b00514
Macromolecules 2015, 48, 3890−3899

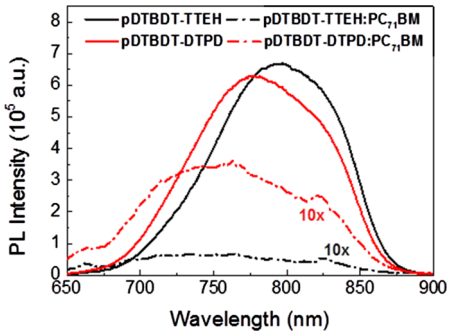

Figure 7. (a) PL spectra of pDTBDT-TTEH, pDTBDT-DTPD, pDTBDT-TTEH:$PC_{71}BM$, and pDTBDT-DTPD:$PC_{71}BM$ films. Blend films were spin-cast from a chlorobenzene solution containing the 3 vol % DIO additive, and the intensities of their raw data were multiplied by 10 to show more clearly.

the pDTBDT-TTEH and $PC_{71}BM$ in CV measurements. In the same manner, the less PL quenching in the pDTBDT-DTPD:$PC_{71}BM$ blend film can be explained by two factors: (i) poor phase separation and (ii) lower LUMO−LUMO offset between the pDTBDT-DTPD and $PC_{71}BM$. In conclusion, crystallinity, morphology, and PL quenching in polymer:$PC_{71}BM$ blend films revealed that the pDTBDT-TTEH:$PC_{71}BM$ blend film has more favorable features for high values in J_{sc} and PCE than the pDTBDT-DTPD:$PC_{71}BM$ blend.

The hole mobilities of polymer:$PC_{71}BM$ blends were determined by the space charge limited current (SCLC) method. Devices with a configuration of ITO/PEDOT:PSS/polymer:$PC_{71}BM$/Au were fabricated and voltages were swept with recording currents in the dark. Figure S7 shows $J-V$ characteristics of the polymer:$PC_{71}BM$ blend films. The hole mobilities of pDTBDT-TTEH:$PC_{71}BM$ and pDTBDT-DTPD:$PC_{71}BM$ films were estimated to be 8.4×10^{-5} and 7.0×10^{-5} cm^2 V^{-1} s^{-1}, respectively. The pDTBDT-TTEH:$PC_{71}BM$ film showed a relatively high hole mobility, accounting for its high J_{sc}, FF, and PCE and suggesting that nanoscale phase-separated polymer domains are well connected.

Besides PCEs, the stability of photovoltaic cells is highly important to their potential commercial value. To test the stability of cells containing our polymers, they were incorporated into inverted-type PSCs, known to be more stable than other structures, fabricated in structures of ITO/TiO_2 or PEIE/polymer:$PC_{71}BM$/MoO_3/Ag. Electron extraction layers (EELs) of titanium oxide (TiO_2)[42] nanoparticles and polyethylenimide, 80% ethoxylated (PEIE)[43] were prepared as described previously. Figure 8 shows the current density−voltage curves of TiO_2/pDTBDT-TTEH, PEIE/pDTBDT-TTEH, and TiO_2/pDTBDT-DTPD devices, and Table 3 summarizes the measured photovoltaic parameters. In general, photovoltaic performances were similar to the normal type devices regardless of the type of EELs. More importantly, the performance of pDTBDT-TTEH and pDTBDT-DTPD devices after storage in air in the dark without encapsulation differed significantly; pDTBDT-TTEH devices were highly stable, whereas pDTBDT-DTPD devices degraded rapidly. The photovoltaic properties of eight devices were averaged. Figure 9 displays the representative current density−voltage curves and a summary of average PCE changes. The initial average PCEs of TiO_2/pDTBDT-TTEH, PEIE/pDTBDT-TTEH, and TiO_2/pDTBDT-DTPD devices were respectively 6.00 ± 0.08, 6.03 ± 0.25, and 4.36 ± 0.09%, which decreased to 5.07 ± 0.34, 5.75 ± 0.12, and 1.37 ± 0.11%, respectively, after 1000 h. Notably, PEIE/pDTBDT-TTEH devices degraded only 5% over 1000 h. The degradation of the TiO_2/pDTBDT-DTPD devices was mainly caused by the loss in J_{sc} and FF. For comparison, inverted-type TiO_2/PTB7 devices, a common standard in the field of PSCs, were also fabricated, and their photovoltaic properties were monitored in the same conditions. ITO/TiO_2/PTB7:$PC_{71}BM$/MoO_3/Ag (TiO_2/PTB7) devices exhibited considerable degradation in performance, specifically 32%. Figure S8 shows the current density curves and PCE changes of TiO_2/PTB7 devices. Initially, these devices performance measured V_{oc} = 0.75 V, J_{sc} = 15. 88 mA/cm^2, FF = 63%, and PCE = 7.52%, while after 980 h, these values decreased to V_{oc} = 0.74 V, J_{sc} = 13.27 mA/cm^2, FF = 52%, and PCE = 5.13%. Here again, the parameters of J_{sc} and FF decreased over time.

Generally, device stability is associated with electrode oxidation, photochemical degradation, and morphological changes in photoactive layers and interfaces.[44−51] Considering that the same interlayers and the same contact electrodes in the TiO_2/pDTBDT-TTEH and TiO_2/pDTBDT-DTPD devices, the electrode oxidation and interfacial layers were less likely responsible for the high stability difference. Because both the devices were stored in the dark, photochemical degradation can be also ruled out. Then, the device performance degradation was most susceptible to morphological changes in the photoactive layer. To confirm this, the surfaces of the aged device films were examined by AFM. Figure S9 shows the AFM images of the device surfaces near Ag electrodes. The TiO_2/

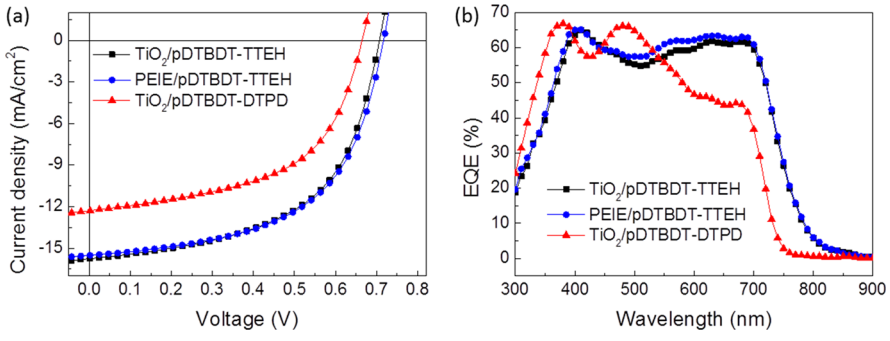

Figure 8. (a) Current density−voltage characteristics of the inverted type pDTBDT-TTEH and pDTBDT-DTPD devices under simulated 100 mW/cm^2 AM1.5G illumination and (b) their EQE spectra. The data shown in black, blue, and red correspond to devices based respectively on the TiO_2/pDTBDT-TTEH:$PC_{71}BM$, PEIE/pDTBDT-TTEH:$PC_{71}BM$, and TiO_2/pDTBDT-DTPD:$PC_{71}BM$ films.

DOI: 10.1021/acs.macromol.5b00514
Macromolecules 2015, 48, 3890−3899

Table 3. PV Performance of the Inverted Polymer:$PC_{71}BM$ Devices

active layer	electron extraction layer	V_{oc} (V)	$J_{SC,I-V}$ (mA/cm^2)	FF (%)	PCE (%)
pDTBDT-TTEH:$PC_{71}BM$	TiO_2	0.71	15.75	55.35	6.16 (av: 6.00)
pDTBDT-TTEH:$PC_{71}BM$	PEIE	0.72	15.51	56.10	6.24 (av: 6.03)
pDTBDT-DTPD:$PC_{71}BM$	TiO_2	0.67	12.29	54.33	4.44 (av: 4.36)

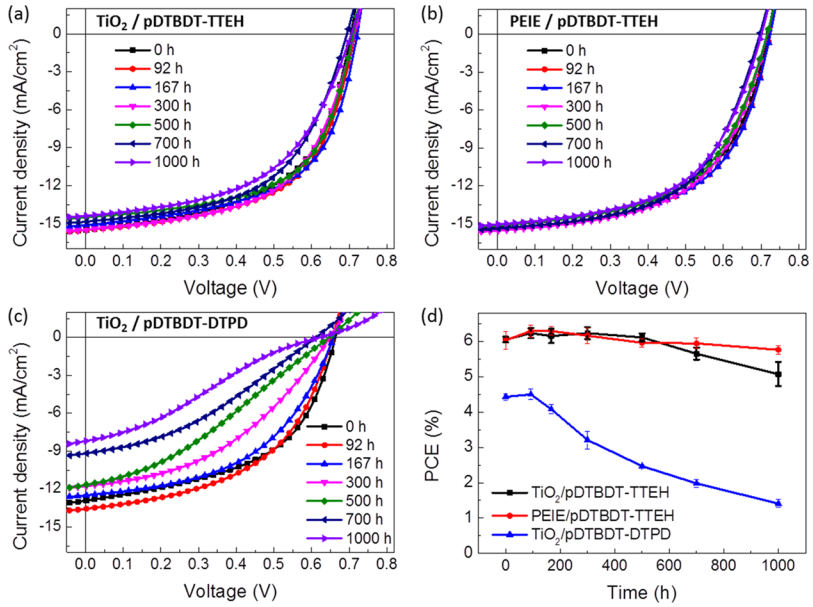

Figure 9. Representative current density−voltage characteristics under simulated 100 mW/cm^2 AM1.5G illumination as a function of storage time: (a) TiO_2/pDTBDT-TTEH:$PC_{71}BM$, (b) PEIE/pDTBDT-TTEH:$PC_{71}BM$, and (c) TiO_2/pDTBDT-DTPD:$PC_{71}BM$ blend films. (b) A summary of PCE degradation over storage time.

pDTBDT-TTEH device displayed similar surfaces to the just-made surface film, whereas the TiO_2/pDTBDT-DTPD device showed severely aggregated surface morphology after storage in air. The strong aggregation in the pDTBDT-DTPD:$PC_{71}BM$ film suggested that the phase-separation had proceeded over time, and at the same time, the poorer contact of pDTBDT-DTPD:$PC_{71}BM$ layer with the interlayers might have developed. The unfavorable morphological change resulted in the significant loss in J_{sc} and the large increase of series resistances in the TiO_2/pDTBDT-DTPD device. Note that the behavior of morphological stability may be strongly associated with film crystallinity because it is expected that the highly networked nanoscopic crystalline domains of polymers and $PC_{71}BM$s can maintain the initial morphology with optimized phase separation as in the case of pDTBDT-TTEH:$PC_{71}BM$ film.

In addition, air infiltration into devices is another important factor to determine device stability. The air-infiltration issue was easily observed from our stability results on encapsulated TiO_2/PTB7 devices (only 10% degradation over 1100 h, Figure S10) versus unencapsulated TiO_2/PTB7 devices (32% degradation as mentioned above). One can expect that air-induced degradation can be deterred by employing highly crystalline films because tightly packed crystalline domains would act as a barrier for air diffusion into the devices. Therefore, the crystallinity of photoactive films would play a critical role in protection of devices from air. This postulation was verified by the comparison of the degradation behavior of the TiO_2/pDTBDT-TTEH, TiO_2/pDTBDT-DTPD, and the TiO_2/PTB7 devices with the initial photoactive film crystallinity. The highly crystalline, nanoscopically connected pDTBDT-TTEH domains in the pDTBDT-TTEH:$PC_{71}BM$ blend films protected the photoactive layer from air-induced degradation better than the less crystalline, aggregated pDTBDT-DTPD domains in the pDTBDT-DTPD:$PC_{71}BM$ blend films; PTB7 in the PTB7:$PC_{71}BM$ films displayed an intermediate crystallinity in between that of pDTBDT-TTEH and pDTBDT-DTPD devices (Figure S11 displays GIXD images obtained from the PTB7 and PTB7:$PC_{71}BM$ films); the degradation of PTB7 devices also lied in between the performance decays of pDTBDT-TTEH and pDTBDT-DTPD devices. In conclusion, the high film crystallinity is beneficial for high device stability because it assists in retaining the initial photoactive film morphology and blocking air infiltration into devices.

4. CONCLUSIONS

We synthesized pDTBDT-TTEH and pDTBDT-DTPD polymers based on a planar fused ring system of DTBDT moieties. The TTEH acceptor produced a linear planar polymer backbone, whereas the DTPD acceptor formed a highly twisted polymer backbone. Both polymers produced a low band gap of about 1.6 eV. The photovoltaic properties of devices based on these polymers were highly distinct: PCE values of 6.75% vs 4.44% for pDTBDT-TTEH- and pDTBDT-DTPD-based devices. At the same time, pDTBDT-TTEH devices were highly stable in air, whereas the performance of pDTBDT-DTPD devices decreased significantly after long storage periods. Film characterizations revealed that the nanoscopically phase-separated crystalline characteristics of the pDTBDT-TTEH:$PC_{71}BM$ blend films afforded the higher PCE and air stability. This work demonstrates that the linear,

DOI: 10.1021/acs.macromol.5b00514
Macromolecules 2015, 48, 3890−3899

long planar polymer backbones are advantageous not only for high photovoltaic performance but also for high device stability.

■ ASSOCIATED CONTENT

Supporting Information

H NMR of compound **1**, compound **2**, compound **3**, and polymers, thermal properties of pDTBDT-TTEH and pDTBDT-DTPD polymers, *J*−*V* curves of pDTBDT-TTEH:$PC_{71}BM$ and pDTBDT-DTPD:$PC_{71}BM$ hole-only devices, TiO_2/PTB7:$PC_{71}BM$ device characteristics, and GIXD data of PTB7 and PTB7:$PC_{71}BM$ films. The Supporting Information is available free of charge on the ACS Publications website at DOI: 10.1021/acs.macromol.5b00514.

■ AUTHOR INFORMATION

Corresponding Authors

*E-mail: skwon@gnu.ac.kr (S.K.).
*E-mail: bongsoo@kist.re.kr (B.K.).
*E-mail: ykim@gnu.ac.kr (Y.K.).

Author Contributions

N.S., H.-J.Y., and Y.Y. contributed equally to this work.

Notes

The authors declare no competing financial interest.

■ ACKNOWLEDGMENTS

This work was supporetd by a grant from the National Reserach Foundation of Korea (NRF) funded by the Korean Goverment (2012R1A2A2A06047047 and 2010-0029084) and by New and Renewable Energy Program of the Korea Institute of Energy Technology Evaluation and Planning (KETEP) grant funded by the Ministry of Knowledge Economy (MKE) (20113030010030 and 20133030000130) and by Korea Institute of Science and Technology (KIST) Internal Programs.

■ REFERENCES

(1) Yu, G.; Gao, J.; Hummelen, J. C.; Wudl, F.; Heeger, A. J. *Science* **1995**, *270*, 1789−1791.
(2) He, Z.; Zhong, C.; Su, S.; Xu, M.; Wu, H.; Cao, Y. *Nat. Photonics* **2012**, *6*, 591−595.
(3) Liu, Y.; Zhao, J.; Li, Z.; Mu, C.; Ma, W.; Hu, H.; Jiang, K.; Lin, H.; Ade, H.; Yan, H. *Nat. Commun.* **2014**, *5*.
(4) Cheng, Y.-J.; Yang, S.-H.; Hsu, C.-S. *Chem. Rev.* **2009**, *109*, 5868−5923.
(5) Servaites, J. D.; Ratner, M. A.; Marks, T. J. *Energy Environ. Sci.* **2011**, *4*, 4410−4422.
(6) Guo, X.; Zhou, N.; Lou, S. J.; Smith, J.; Tice, D. B.; Hennek, J. W.; Ortiz, R. P.; Navarrete, J. T. L.; Li, S.; Strzalka, J.; Chen, L. X.; Chang, R. P. H.; Facchetti, A.; Marks, T. J. *Nat. Photonics* **2013**, *7*, 825−833.
(7) Osaka, I.; Kakara, T.; Takemura, N.; Koganezawa, T.; Takimiya, K. *J. Am. Chem. Soc.* **2013**, *135*, 8834−8837.
(8) Tumbleston, J. R.; Collins, B. A.; Yang, L.; Stuart, A. C.; Gann, E.; Ma, W.; You, W.; Ade, H. *Nat. Photonics* **2014**, *8*, 385−391.
(9) Lu, L.; Xu, T.; Chen, W.; Landry, E. S.; Yu, L. *Nat. Photonics* **2014**, *8*, 716−722.
(10) Chen, H.-Y.; Hou, J.; Zhang, S.; Liang, Y.; Yang, G.; Yang, Y.; Yu, L.; Wu, Y.; Li, G. *Nat. Photonics* **2009**, *3*, 649−653.
(11) Kim, S.-O.; Kim, Y.-S.; Yun, H.-J.; Kang, I.; Yoon, Y.; Shin, N.; Son, H. J.; Kim, H.; Ko, M. J.; Kim, B.; Kim, K.; Kim, Y.-H.; Kwon, S.-K. *Macromolecules* **2013**, *46*, 3861−3869.
(12) You, J.; Dou, L.; Yoshimura, K.; Kato, T.; Ohya, K.; Moriarty, T.; Emery, K.; Chen, C.-C.; Gao, J.; Li, G.; Yang, Y. *Nat. Commun.* **2013**, *4*, 1446.
(13) Zhang, Z.-G.; Li, Y. *Sci. China Chem.* **2015**, *58*, 192−209.
(14) Huo, L.; Zhang, S.; Guo, X.; Xu, F.; Li, Y.; Hou, J. *Angew. Chem., Int. Ed.* **2011**, *50*, 9697−9702.
(15) Li, Y. *Acc. Chem. Res.* **2012**, *45*, 723−733.
(16) Faist, M. A.; Kirchartz, T.; Gong, W.; Ashraf, R. S.; McCulloch, I.; de Mello, J. C.; Ekins-Daukes, N. J.; Bradley, D. D. C.; Nelson, J. *J. Am. Chem. Soc.* **2011**, *134*, 685−692.
(17) Janssen, R. A. J.; Nelson, J. *Adv. Mater.* **2013**, *25*, 1847−1858.
(18) Clarke, T. M.; Durrant, J. R. *Chem. Rev.* **2010**, *110*, 6736−6767.
(19) Kim, J.-H.; Park, J. B.; Xu, F.; Kim, D.; Kwak, J.; Grimsdale, A. C.; Hwang, D.-H. *Energy Environ. Sci.* **2014**, *7*, 4118−4131.
(20) Brabec, C. J.; Gowrisanker, S.; Halls, J. J. M.; Laird, D.; Jia, S.; Williams, S. P. *Adv. Mater.* **2010**, *22*, 3839−3856.
(21) Ye, L.; Zhang, S.; Zhao, W.; Yao, H.; Hou, J. *Chem. Mater.* **2014**, *26*, 3603−3605.
(22) Cui, C.; Wong, W.-Y.; Li, Y. *Energy Environ. Sci.* **2014**, *7*, 2276−2284.
(23) Lee, J.; Jo, S. B.; Kim, M.; Kim, H. G.; Shin, J.; Kim, H.; Cho, K. *Adv. Mater.* **2014**, *26*, 6706−6714.
(24) Liang, Y.; Yu, L. *Acc. Chem. Res.* **2010**, *43*, 1227−1236.
(25) Son, H. J.; Wang, W.; Xu, T.; Liang, Y.; Wu, Y.; Li, G.; Yu, L. *J. Am. Chem. Soc.* **2011**, *133*, 1885−1894.
(26) Li, W.; Roelofs, W. S. C.; Wienk, M. M.; Janssen, R. A. J. *J. Am. Chem. Soc.* **2012**, *134*, 13787−13795.
(27) Huang, Y.; Huo, L.; Zhang, S.; Guo, X.; Han, C. C.; Li, Y.; Hou, J. *Chem. Commun.* **2011**, *47*, 8904−8906.
(28) Najari, A.; Beaupré, S.; Berrouard, P.; Zou, Y.; Pouliot, J.-R.; Lepage-Pérusse, C.; Leclerc, M. *Adv. Funct. Mater.* **2011**, *21*, 718−728.
(29) Cheon, Y. R.; Kim, Y. J.; Ha, J.-j.; Kim, M.-J.; Park, C. E.; Kim, Y.-H. *Macromolecules* **2014**, *47*, 8570−8577.
(30) Son, H. J.; Lu, L.; Chen, W.; Xu, T.; Zheng, T.; Carsten, B.; Strzalka, J.; Darling, S. B.; Chen, L. X.; Yu, L. *Adv. Mater.* **2013**, *25*, 838−843.
(31) Biniek, L.; Schroeder, B. C.; Donaghey, J. E.; Yaacobi-Gross, N.; Ashraf, R. S.; Soon, Y. W.; Nielsen, C. B.; Durrant, J. R.; Anthopoulos, T. D.; McCulloch, I. *Macromolecules* **2013**, *46*, 727−735.
(32) Ashraf, R. S.; Meager, I.; Nikolka, M.; Kirkus, M.; Planells, M.; Schroeder, B. C.; Holliday, S.; Hurhangee, M.; Nielsen, C. B.; Sirringhaus, H.; McCulloch, I. *J. Am. Chem. Soc.* **2015**, *137*, 1314−1321.
(33) Zhong, H.; Li, Z.; Deledalle, F.; Fregoso, E. C.; Shahid, M.; Fei, Z.; Nielsen, C. B.; Yaacobi-Gross, N.; Rossbauer, S.; Anthopoulos, T. D.; Durrant, J. R.; Heeney, M. *J. Am. Chem. Soc.* **2013**, *135*, 2040−2043.
(34) Hutchison, G. R.; Ratner, M. A.; Marks, T. J. *J. Am. Chem. Soc.* **2005**, *127*, 2339−2350.
(35) Coropceanu, V.; Cornil, J.; da Silva Filho, D. A.; Olivier, Y.; Silbey, R.; Brédas, J.-L. *Chem. Rev.* **2007**, *107*, 926−952.
(36) Zade, S. S.; Zamoshchik, N.; Bendikov, M. *Acc. Chem. Res.* **2010**, *44*, 14−24.
(37) Yun, H.-J.; Lee, Y.-J.; Yoo, S.-J.; Chung, D. S.; Kim, Y.-H.; Kwon, S.-K. *Chem.—Eur. J.* **2013**, *19*, 13242−13248.
(38) Piliego, C.; Holcombe, T. W.; Douglas, J. D.; Woo, C. H.; Beaujuge, P. M.; Fréchet, J. M. J. *J. Am. Chem. Soc.* **2010**, *132*, 7595−7597.
(39) Chen, W.; Xu, T.; He, F.; Wang, W.; Wang, C.; Strzalka, J.; Liu, Y.; Wen, J.; Miller, D. J.; Chen, J.; Hong, K.; Yu, L.; Darling, S. B. *Nano Lett.* **2011**, *11*, 3707−3713.
(40) Huang, Y.; Guo, X.; Liu, F.; Huo, L.; Chen, Y.; Russell, T. P.; Han, C. C.; Li, Y.; Hou, J. *Adv. Mater.* **2012**, *24*, 3383−3389.
(41) Wu, Y.; Li, Z.; Ma, W.; Huang, Y.; Huo, L.; Guo, X.; Zhang, M.; Ade, H.; Hou, J. *Adv. Mater.* **2013**, *25*, 3449−3455.
(42) Chung, W.-S.; Lee, H.; Lee, W.; Ko, M. J.; Park, N.-G.; Ju, B.-K.; Kim, K. *Org. Electron.* **2010**, *11*, 521−528.
(43) Zhou, Y.; Fuentes-Hernandez, C.; Shim, J.; Meyer, J.; Giordano, A. J.; Li, H.; Winget, P.; Papadopoulos, T.; Cheun, H.; Kim, J.; Fenoll, M.; Dindar, A.; Haske, W.; Najafabadi, E.; Khan, T. M.; Sojoudi, H.; Barlow, S.; Graham, S.; Brédas, J.-L.; Marder, S. R.; Kahn, A.; Kippelen, B. *Science* **2012**, *336*, 327−332.

DOI: 10.1021/acs.macromol.5b00514
Macromolecules 2015, 48, 3890−3899

(44) Jørgensen, M.; Norrman, K.; Gevorgyan, S. A.; Tromholt, T.; Andreasen, B.; Krebs, F. C. *Adv. Mater.* **2012**, *24*, 580−612.
(45) Tournebize, A.; Bussière, P.-O.; Wong-Wah-Chung, P.; Thérias, S.; Rivaton, A.; Gardette, J.-L.; Beaupré, S.; Leclerc, M. *Adv. Energy Mater.* **2013**, *3*, 478−487.
(46) Aygül, U.; Hintz, H.; Egelhaaf, H.-J.; Distler, A.; Abb, S.; Peisert, H.; Chassé, T. *J. Phys. Chem. C* **2013**, *117*, 4992−4998.
(47) Zhang, H.; Borgschulte, A.; Castro, F. A.; Crockett, R.; Gerecke, A. C.; Deniz, O.; Heier, J.; Jenatsch, S.; Nüesch, F.; Sanchez-Sanchez, C.; Zoladek-Lemanczyk, A.; Hany, R. *Adv. Energy Mater.* **2015**, *5*, 1400734.
(48) Hoke, E. T.; Sachs-Quintana, I. T.; Lloyd, M. T.; Kauvar, I.; Mateker, W. R.; Nardes, A. M.; Peters, C. H.; Kopidakis, N.; McGehee, M. D. *Adv. Energy Mater.* **2012**, *2*, 1351−1357.
(49) Peters, C. H.; Sachs-Quintana, I. T.; Kastrop, J. P.; Beaupré, S.; Leclerc, M.; McGehee, M. D. *Adv. Energy Mater.* **2011**, *1*, 491−494.
(50) Peters, C. H.; Sachs-Quintana, I. T.; Mateker, W. R.; Heumueller, T.; Rivnay, J.; Noriega, R.; Beiley, Z. M.; Hoke, E. T.; Salleo, A.; McGehee, M. D. *Adv. Mater.* **2012**, *24*, 663−668.
(51) Distler, A.; Kutka, P.; Sauermann, T.; Egelhaaf, H.-J.; Guldi, D. M.; Di Nuzzo, D.; Meskers, S. C. J.; Janssen, R. A. J. *Chem. Mater.* **2012**, *24*, 4397−4405.

DOI: 10.1021/acs.macromol.5b00514
Macromolecules 2015, 48, 3890−3899